American Mineralogist, Volume 90, pages 695–700, 2005

Low-*T* neutron powder-diffraction and synchrotron-radiation IR study of synthetic amphibole $Na(NaMg)Mg_5Si_8O_{22}(OH)_2$

G. IEZZI,[1,*] G.D. GATTA,[1] W. KOCKELMANN,[2] G. DELLA VENTURA,[3] R. RINALDI,[4] W. SCHÄFER,[5] M. PICCININI,[6] AND F. GAILLARD[1]

[1]Bayerisches Geoinstitut, Universität Bayreuth, D-95440 Bayreuth, Germany
[2]ISIS, Rutherford Appleton Laboratory, Chilton, Didcot, U.K.
[3]Dipartimento di Scienze Geologiche, Università di Roma Tre, Largo S. Leonardo, Roma, Italy
[4]Dipartimento di Scienze della Terra, Università di Perugia, Italy
[5]Forschungszentrum Jülich, D-52425 Jülich, Germany
[6]Laboratori Nazionali di Frascati, I.N.F.N., Frascati, Italy

ABSTRACT

$^{A}Na^{B}(NaMg)^{C}Mg_5Si_8O_{22}(OH,D)_2$ amphibole was hydrothermally synthesized at 850 °C and 0.3 GPa. SEM, EPMA, and X-ray powder-diffraction data showed the experimental product to consist of a high amphibole yield (90–95%), plus minor quartz and rare enstatite. Neutron powder-diffraction data were collected using a time-of-flight diffractometer at room *T* and at 8 K, respectively, and structure refinement was carried out using the Rietveld method. The space group of the amphibole is $P2_1/m$ at both temperatures, as confirmed by the presence of *b*-type reflections ($h + k = 2n + 1$). FTIR OH- and OD-stretching spectra at both room and low *T* (30 K) show two main absorptions, which are assigned to two non-equivalent OH groups in the structure, and a third lower-frequency band, assigned to A-site vacant environments (local cummingtonite environments). At room- and low-*T*, the cell parameters are (in Å): *a* 9.7188(1) and 9.7016(2), *b* 17.9385(3) and 17.8953(4), *c* 5.2692(1) and 5.2574(1); β (°) is 102.526(1) and 102.597(2). Cell volumes (Å^3) are 896.78(2) at room *T* and 890.80(2) at 8 K, with a relative reduction of less than 1%. Accurate structural positions for the hydrogen atoms were obtained from diffraction data. The O5A-O6A-O5A and O5B-O6B-O5B angles, diagnostic of the A- and B-chains kinking along **c**, are 190.0° and 159.2° at 293 K and 193.8° and 156.8° at 8 K, respectively. The orientation of the thermoelastic strain ellipsoid was calculated and the principal unit-strain tensor components are reported. A comparison between the low-temperature data reported here and the high-temperature data for a similar amphibole composition, reported by Cámara et al. (2003) up to 643 K, is discussed.

INTRODUCTION

Many studies of amphiboles and pyroxenes have been done at non-ambient *T* and *P* conditions (see Yang and Prewit 2000 for a list of references). Accordingly, most of the high-temperature (HT) and high-pressure (HP) phase transitions for monoclinic pyroxenes and amphiboles involve transformations between *P*- and *C*-centered lattices (Arlt and Angel 2000; Cámara et al. 2003 and references therein). In the *P* lattice, the facing chains of tetrahedra (generally labeled "A" and "B" chains, e.g., Hawthorne 1983) are non-equivalent; by contrast, in the *C*-centered lattice, the facing chains are symmetrically equivalent. The phase transitions in both mineral groups are driven by the relative volume modifications (expansion and/or contraction) occurring within the octahedral and tetrahedral portions of their structures as a function of *T* and *P* (see Yang and Prewit 2000 and references therein). As a first approximation, single tetrahedra behave as rigid units during deformation, and the tetrahedral chains respond to changes in *T* and *P* by kinking through rotations (O- and/or S-type rotation) around the [100] axis (Thompson 1970; Yang and Prewitt 2000). By contrast, the M octahedra show significant modifications of the polyhedron volumes and may also change their coordination number (i.e., M2 for clinopyroxenes and M4 for clinoamphiboles) across a phase transition. The degree of chain kinking is indicated by the O3-O3-O3 angle for clinopyroxene and by the O5-O6-O5 angle for clinoamphiboles (Yang and Prewit 2000; Arlt and Angel 2000; Cámara et al. 2003 and references therein).

In general, the structural evolution of chain silicates under LT, HT, and HP conditions gives rise to anisotropic thermoelastic changes (Yang and Prewit 2000; Origlieri et al. 2003). The structural changes found in clinopyroxenes under non-ambient conditions support the idea that three polymorphs may exist for a fixed composition: *C*(HT) → *P* → *C*(HP) (Arlt and Angel 2000) where *C* and *P* stand for centered and primitive lattice, respectively. The HT-C phases have extended and equivalent tetrahedral chains, whereas the HP-C phases have strongly corrugated chains. The intermediate *P*-lattice polymorph has one chain similar to the *C*(HT)- and one similar to the *C*(HP)-polymorph (Arlt and Angel 2000).

* Presently address: Dipartimento di Scienze della Terra, Università G. D'Annunzio, I-66013 Chieti Scalo, Italy. E-mail: g.iezzi@unich.it

0003-004X/05/0004–695$05.00/DOI: 10.2138/am.2005.1764

Although much is known about chain silicates at high *T* and *P*, few data are available at low-*T* cryogenic conditions. A few studies of Li-bearing pyroxenes have been reported (Tribaudino et al. 2003; Redhammer et al. 2001; Sato et al. 1995 and references therein). By contrast, for amphiboles, to the best of our knowledge, only one study has been reported at low *T* (140 K), by Yang and Smyth (1996) on cummingtonite.

The synthetic amphibole $Na(NaMg)Mg_5Si_8O_{22}(OH)_2$ (Cámara et al. 2003; Iezzi et al. 2004) is an excellent candidate for LT structural investigation. It has $P2_1/m$ symmetry at room *T*, like Mg-rich cummingtonite, $(Mg,Fe^{2+})_7Si_8O_{22}(OH)_2$, but has several peculiar features: (1) two cations, one mono- and one divalent, with very different sizes, at the M4 site; (2) a fully occupied A-site; and (3) a rather ordered structure, with only Si at the T-sites and Mg at the C-sites. Like cummingtonite, the A and B double-chains have S and O rotations, respectively; however, the degrees of kinking of the A and B double-chains are, respectively, the largest and the smallest so far reported for $P2_1/m$ amphiboles (Cámara et al. 2003). The HT-behavior of such an amphibole has recently been investigated by Cámara et al. (2003), who observed a $P2_1/m \rightarrow C2/m$ displacive phase-transition at about 527 K.

We report here an in situ LT study of synthetic $NaNaMgMg_5Si_8O_{22}(OH)_2$ by neutron powder diffraction and synchrotron IR spectroscopy. The aim of this study is to characterize the deformation dynamics and the thermoelastic behavior at low temperature and to investigate the possible existence of a low-*T* phase-transition [i.e., $P2_1/m \rightarrow C2/m$(LT)] in this amphibole. The quality of the neutron data is much higher than those obtained by powder X-ray diffraction of synthetic amphiboles. This is due primarily to the fact that neutrons are scattered by nuclei which, compared with electron orbitals, are point scatterers. Hence powder neutron-diffraction can provide very accurate data for atomic parameters and bond lengths, especially for O-H groups in the $P2_1/m$ structure (Rinaldi 2002). Refinement results are comparable to those obtained by SC-XRD. The requirement for a relatively large sample size (2–3 g) in neutron experiments may be outweighed by the prospect of being able to work on amphiboles synthesized below the *solidus* that are well constrained in terms of their growth conditions compared with those grown from melts for single-crystal X-ray studies.

Experimental methods

The amphibole sample was synthesized at the Bayerisches Geoinstitut using an internally heated vessel pressurized with pure Ar, at 1123 K and 0.3 GPa (Gaillard 2004). The starting material was obtained by melting at room *P* a stoichiometric mixture of oxides. Electron probe micro-analysis (EPMA) showed the glass to be homogeneous and on composition. A portion of finely ground glass was sealed in a Pt tube with the addition of 20 wt% D_2O. Synthesis duration was 48 h; the temperature was controlled with three type-K thermocouples placed around the hot spot, providing an accuracy of 10 K. Rapid cooling was achieved by switching off the power supply; the estimated cooling rate was around 150 K/s.

The synthesis product was studied by X-ray powder diffraction, SEM, and EPMA. The X-ray powder-pattern was collected with a Siemens D5000 diffractometer and was fully indexed in $P2_1/m$ symmetry using GSAS (Larson and Von Dreele 1997), starting from the structural model of Iezzi et al. (2004).

A few milligrams of powder were embedded in epoxy resin and polished. SEM-EDS analysis was done with a Leo-Gemini electron microscope equipped with an OXFORD EDS detector. EPMA was also carried out in the WDS mode with a CAMECA SX-50 microprobe operating at 15 kV excitation voltage, 8 nA beam current, 20 s counting time on peak and 10 s counting time on background. The standards used were albite (TAP) for Na and Si and enstatite (TAP) for Mg; data reduction for quantitative analysis was done with the PAP method (Pouchou and Pichoir 1985).

Synchrotron-radiation FTIR spectra were collected at SINBAD, the new synchrotron IR radiation facility at the Laboratori Nazionali di Frascati of I.N.F.N. Samples were prepared as KBr pellets, with a dilution of 5 wt% (Della Ventura et al. 1996). Powder FTIR OH-stretching spectra (4000–2500 cm^{-1}) were collected at the IR synchrotron beam line using a Bruker Equinox 55 interferometer modified to work in vacuum. Spectra in the medium IR frequency range were acquired, covering both the O-D and the O-H stretching regions, with a resolution of 4 cm^{-1}. Two spectra were recorded, one at room temperature (298 K) and one at 20 K, using a liquid-helium cryostat.

Description of the sample

A powder consisting of > 95% amphibole (from Rietveld analysis of the powder pattern and SEM/EDS observations) plus quartz was obtained. Amphibole crystals (Fig. 1) are acicular and prismatic along **c**, with an average dimension between 10 μm and 40 μm in length and 2–10 μm across; a few crystals up to 150 × 25 μm were observed. Table 1 shows the EPMA data and the X-ray refined room-*T* cell-dimensions for the synthesized amphibole. The crystal chemical formula, based on 24 oxygen atoms, assuming T = 8 Si apfu and O(H,D) = 2 apfu, is $(Na_{0.92}\square_{0.08})(Na_{0.92}Mg_{1.08})Mg_5Si_8O_{22}(OH,D)_2$. This composition is identical to that of sample 351 synthesized at 1123 K and 0.4 GPa by Iezzi et al. (2004).

Neutron-diffraction data collection and Rietveld structure refinement

Neutron powder-diffraction data were collected using the ROTAX time-of-flight (TOF) diffractometer installed at the pulsed spallation source ISIS of the Rutherford Appleton Laboratory, U.K. The instrument uses a "white" beam with neutron wavelengths between 0.7–5.1 Å. The primary flight path is 14.0 m. The amphibole powder sample was packed into an 8 mm diameter vanadium can. Diffraction patterns were collected at 297 K using three fixed-angle detector banks at 2θ scattering angles of 29.1, 72.8, and 122.0°, respectively (Table 2). For low-temperature data collections at 8 K, the sample, contained in the vanadium can, was placed inside the vanadium cell of a closed-cycle refrigerator cryostat. The cell was filled with He gas to facilitate heat exchange between the cold surface of

Table 1. Chemical composition, crystal-chemical formula (based on 24 O and 8 Si apfu) and cell parameters (Rietveld refinement of powder XRD data at room-*T*)

Chemical composition			Cell parameters		
SiO_2	60.03 (0.23)	Si	8.00	*a* (Å)	9.7167 (3)
MgO	30.6 (0.28)	Mg	6.08	*b* (Å)	17.9308 (5)
Na_2O	7.12 (0.16)	Na	1.84	*c* (Å)	5.2685 (2)
Total	97.75 (0.22)	O(H,D)	2.00	β (°)	102.539 (3)
				V (Å^3)	896.027(52)

Figure 1. SEM image of the studied powder. The scale bar is 40 μm.

the cryostat and the sample container.

Rietveld structure refinements of the spectra from all three detector banks were done simultaneously using GSAS (Larson and Von Dreele 1997); the starting model was that obtained at room *T* by Cámara et al. (2003). The neutron-scattering lengths were taken from the GSAS library. Scale factor, background (modeled by Chebyschev polynomials with different sets of coefficients for the three banks), zero shift, cell parameters, and peak-profile were refined first. The time-of-flight peak-shape parameters were fitted with a double exponential pseudo-Voigt function. Then the atom parameters (positions, occupancies, and thermal displacements) were refined.

All atoms were refined isotropically; thermal parameters were refined by grouping them on the basis of their environment and constraining the same shift within each group (Table 2). The C- and T-sites were considered completely occupied by Mg and Si, respectively. In contrast, Na and Mg at the B site were refined starting with values derived from the EPMA and IR data. ^{A}Na and ^{B}Na were constrained to be equal during the refinement. The populations of hydrogen and deuterium at the H1 and H2 sites were also refined.

Stereochemical restraints were introduced for the bond distances to avoid divergence in the first cycles of refinement. The statistical weight of these restraints was gradually decreased to zero as the refinement proceeded. The preferred-orientation correction along the diffraction vector [001], using the Dollase-March formulation (Dollase 1986), was applied. However, despite the fibrous habit of the amphibole, a very small correction was needed, as shown by the value of the coefficient R_0, which is close to 1 (0.9). Absorption caused by the sample, the vanadium container, and vanadium cryostat walls was accounted for by fitting one linear-absorption parameter common to the three ROTAX histograms. At the end of the refinement, the shifts in all parameters were less than their standard deviations. Observed and calculated diffraction spectra are shown in Figure 2 for both the 298 and 8 K data collections. Further details of the structural refinements are reported in Table 2. Tables 3 and 4 give the refined structure parameters and selected bond lengths at 298 and 8 K, respectively.

TABLE 2. Neutron powder-diffraction data collection and refinement

	T = 293 K	*T* = 8 K
Crystal system	Monoclinic	Monoclinic
Space group; (*Z* = 2)	*P* 2$_1$/*m*	*P* 2$_1$/*m*
Cell parameters		
a (Å)	9.71887(15)	9.70169(17)
b (Å)	17.93853(31)	17.89537(36)
c (Å)	5.26923(9)	5.25744(10)
β (°)	102.526(1)	102.597(2)
V (Å^3)	896.782(16)	890.800(20)
ρ$_{calc}$/g cm^{-3}	2.963	2.983
Reduction of cell parameter (Δ 298 to 8K)	absolute	%
Δ *a* (Å)	0.172	0.18
Δ *b* (Å)	0.431	0.24
Δ *c* (Å)	0.117	0.22
Δ β (°)	–0.07	~0.07
Δ *V* (Å^3)	5.982	~0.7
Instrumental settings and goodness of fit		
Bank 1 (forward scattering)		
2θ (°) (center/range)	29.1 / 12–45	
d-spacing coverage (Å)	1.5–20	
No. of data points	1103	1306
R_p*	0.0233	0.0237
R_{wp} †	0.0220	0.0195
R_F2 ‡	0.0460	0.0481
Bank 2 (forward scattering)		
2θ (°) (center/range)	72.8 / 57–87	
d-spacing coverage (Å)	0.65–4	
No. of data points	1816	1816
R_p*	0.0186	0.0191
R_{wp} †	0.0207	0.0207
R_F2 ‡	0.0588	0.0568
Bank 3 (backscattering)		
2θ (°) (center/range)	122.0 / 100–143	
d-spacing coverage (Å)	0.3–3.2	
No. of data points	1615	1599
R_p*	0.0167	0.0175
R_{wp} †	0.0161	0.0171
R_F2 ‡	0.0379	0.0484
Totals		
No. of data points	4534	4721
R_p*	0.0176	0.0184
R_{wp} †	0.0177	0.0180
χ §	4.785	3.672
Refined structural parameters	79	78
Profile + background	6 + 14	6 + 14
Cell parameters	4	4

* $R_p = \Sigma|y_{obs} - y_{calc}|/\Sigma y_{obs}$.
† $R_{wp} = [\Sigma w(y_{obs} - y_{calc})^2/\Sigma w y_{obs}^2]^{1/2}$.
‡ $R_F2 = \Sigma|F_{obs}^2 - F_{calc}^2|/\Sigma|F_{obs}^2|$.
§ $\chi = [\Sigma\, w(y_{obs} - y_{calc})^2 / (N_{obs} - N_{var})]^{1/2}$.

Synchrotron-radiation IR (SR-IR) spectroscopy

The SR-IR spectra (Fig. 3) confirm the presence of both OH and OD groups in the amphibole, in agreement with the neutron structural data. The OH-stretching spectrum at room-*T* (Fig. 3a) is identical to that of sample 351 in Iezzi et al. (2004) with composition $(Na_{0.93}\square_{0.07})$ $(Na_{0.94}Mg_{1.06})$ Mg_5 Si_8 O_{22} $(OH)_2$ and $P2_1/m$ symmetry. The A and B bands are assigned to two non-equivalent O-H groups in the $P2_1/m$ structure, locally interacting with ^{A}Na (Iezzi et al. 2004). The minor C band is assigned to local configurations involving vacant A-sites (cummingtonite configuration), in agreement with the chemical composition derived by EPMA. As expected, the O-D stretching spectrum at room-*T* is identical to the O-H spectrum and is displaced to a lower frequency by a factor $\Delta_{\upsilon OH/\upsilon OD} = 1.36$, which is very close to the value calculated from the ratio of the reduced masses of the O-H/O-D couples. The OH and OD spectra obtained at 300 and 20 K are very similar, in agreement with the fact that both samples have the same symmetry; the only notable effect of *T* is a shift toward higher frequency of the A band (by ~15 cm^{-1}) and a very minor shift toward lower frequencies (by < 5 cm^{-1}) of the B band; the C band remains practically constant.

DISCUSSION

The first interesting result of this study is that the symmetry of the examined amphibole is not modified at low temperature: at 8 K, the lattice is still primitive, as confirmed by the presence

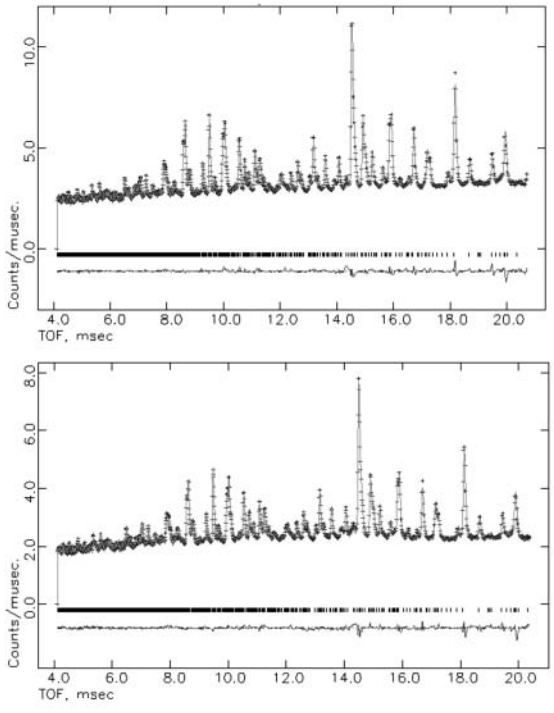

FIGURE 2. TOF neutron powder-diffraction spectra at room *T* (above) and 8 K (below). The crosses are the observed data, the line is the calculated Rietveld fit. Vertical markers = calculated reflections of both amphibole and quartz. The residual between observed and calculated patterns is shown at the bottom.

TABLE 3. Atomic positions, occupancies and isotropic-displacement parameters

Site	*x*		*y*		*z*		Site occup.	U_{iso}	
	298 K	8K	298 K	8 K	298 K	8 K		298 K	8 K
O1A	−0.13689(3)	−0.13735(3)	0.33642(2)	0.33691(2)	0.19974(4)	0.19646(2)	1.00	0.00545(9)	0.00357(8)
O1B	0.36433(2)	0.36675(2)	0.83681(3)	0.83608(3)	0.21721(3)	0.22068(2)	1.00	0.00545(9)	0.00357(8)
O2A	−0.13270(3)	−0.13335(3)	0.42159(3)	0.42242(2)	0.70449(4)	0.70321(4)	1.00	0.00545(9)	0.00357(8)
O2B	0.37237(4)	0.37525(1)	0.92224(2)	0.91974(2)	0.74352(2)	0.74919(2)	1.00	0.00545(9)	0.00357(8)
O3A	−0.14897(3)	−0.15111(2)	0.25	0.25	0.69317(2)	0.70244(3)	1.00	0.00545(9)	0.00357(8)
O3B	0.35927(4)	0.35997(4)	0.75	0.75	0.72024(2)	0.71712(2)	1.00	0.00545(9)	0.00357(8)
O4A	0.11586(3)	0.11908(2)	0.50067(3)	0.49933(2)	0.79981(4)	0.80839(3)	1.00	0.00545(9)	0.00357(8)
O4B	0.63000(2)	0.63160(2)	0.99316(3)	0.99345(3)	0.76836(2)	0.77154(2)	1.00	0.00545(9)	0.00357(8)
O5A	0.09732(3)	0.09694(3)	0.36704(4)	0.36393(2)	0.02195(3)	0.01295(2)	1.00	0.00545(9)	0.00357(8)
O5B	0.59913(4)	0.60373(2)	0.88482(2)	0.88605(3)	0.09577(3)	0.10438(2)	1.00	0.00545(9)	0.00357(8)
O6A	0.09833(3)	0.09837(2)	0.37993(3)	0.38166(2)	0.53135(2)	0.52814(3)	1.00	0.00545(9)	0.00357(8)
O6B	0.59665(4)	0.59421(3)	0.85784(2)	0.85628(3)	0.60458(2)	0.61049(2)	1.00	0.00545(9)	0.00357(8)
O7A	0.08949(2)	0.08616(4)	0.25	0.25	0.30087(4)	0.30292(3)	1.00	0.00545(9)	0.00357(8)
O7B	0.58745(5)	0.58935(2)	0.75	0.75	0.26427(2)	0.26556(2)	1.00	0.00545(9)	0.00357(8)
T1A	0.03422(2)	0.03609(1)	0.33480(1)	0.33535(2)	0.25975(3)	0.25812(1)	1.00	0.00243(9)	0.00328(11)
T1B	0.53040(2)	0.53071(1)	0.83483(2)	0.83565(1)	0.29506(2)	0.30186(2)	1.00	0.00243(9)	0.00328(11)
T2A	0.03285(2)	0.03892(2)	0.42143(1)	0.42099(2)	0.77063(2)	0.76004(2)	1.00	0.00243(9)	0.00328(11)
T2B	0.54682(3)	0.54552(1)	0.91992(2)	0.91791(1)	0.80318(2)	0.80965(1)	1.00	0.00243(9)	0.00328(11)
M1	−0.24026(3)	−0.24280(2)	0.33930(2)	0.33860(3)	0.49828(4)	0.48952(2)	1.00	0.0111(12)	0.00688(15)
M2	−0.25348(2)	−0.25451(3)	0.43071(4)	0.43158(2)	0.98116(4)	0.97520(3)	1.00	0.0111(12)	0.00688(15)
M3	−0.25237(4)	−0.25442(2)	0.25	0.25	0.97893(5)	0.95277(2)	1.00	0.0111(12)	0.00688(15)
M4	−0.25268(4)	−0.24565(2)	0.50848(4)	0.50741(4)	0.48420(4)	0.48160(2)	0.68(3)	0.0111(12)	0.00688(15)
M4′	−0.26475(4)	−0.27291(5)	0.52501(5)	0.52696(3)	0.49913(5)	0.50151(4)	0.29(4)	0.0111(12)	0.00688(15)
A	0.26338(6)	0.26461(4)	0.25	0.25	0.07195(5)	0.06038(4)	0.90	0.0389(15)	0.00688(15)
H1/D1	−0.04703(3)	−0.04591(2)	0.25	0.25	0.75663(3)	0.75809(3)	0.71/0.29	0.0389(15)	0.00688(15)
H2/D2	0.53670(2)	0.53612(2)	0.25	0.25	0.21170(3)	0.21111(2)	0.66/0.34	0.0389(15)	0.00688(15)

TABLE 4. Selected interatomic distances (Å) and angles (°)

	298 K	8 K		298 K	8 K
T1A-O1A	1.6243(3)	1.6429(3)	T1B-O1B	1.5771(3)	1.5545(3)
T1A-O5A	1.6168(4)	1.6135(4)	T1B-O5B	1.6301(2)	1.6474(2)
T1A-O6A	1.6447(2)	1.6410(2)	T1B-O6B	1.6702(3)	1.6469(3)
TiA-O7A	1.6122(2)	1.6045(4)	T1B-O7B	1.6397(2)	1.6604(3)
<T1A-O>	1.6245	1.6255	<T1B-O>	1.6293	1.6273
T2A-O2A	1.5708(3)	1.6326(2)	T2B-O2B	1.6565(3)	1.6130(3)
T2A-O4A	1.6252(2)	1.5964(2)	T2B-O4B	1.5740(2)	1.6243(4)
T2A-O5A	1.6548(4)	1.6737(4)	T2B-O5B	1.6407(3)	1.6319(3)
T2A-O6A	1.7020(2)	1.6189(2)	T2B-O6B	1.6702(2)	1.6588(2)
<T2A-O>	1.6382	1.6304	<T2B-O>	1.6353	1.6320
M1-O1A	2.0425(4)	2.0270(5)	M2-O1A	2.2147(5)	2.2222(4)
M1-O1B	2.1184(5)	2.1374(6)	M2-O1B	2.1452(6)	2.1629(5)
M1-O2A	1.9899(4)	2.0295(5)	M2-O2A	2.0669(4)	2.0461(4)
M1-O2B	2.1855(6)	2.1520(4)	M2-O2B	2.0469(5)	2.0633(6)
M1-O3A	2.0031(5)	2.0308(5)	M2-O4A	1.9916(7)	1.9742(4)
M1-O3B	2.1569(7)	2.1090(8)	M2-O4B	1.9632(5)	1.9108(3)
<M1-O>	2.0827	2.0809	<M2-O>	2.0714	2.0632
M3-O1A (×2)	2.1095(4)	2.1715(4)	$<^{[8]}$A-O>	2.6879	2.6720
M3-O1B (×2)	2.0468(3)	1.9896(4)	O3A-H1	0.9746(5)	0.9985(5)
M3-O3A	1.9832(5)	1.8199(6)	O3B-H2	0.9967(4)	0.9964(4)
M3-O3B	2.0752(6)	2.1990(4)	O5A-O6A-O5A	190.042(9)	193.792(5)
<M3-O>	2.0618	2.0568	O5B-O6B-O5B	159.151(8)	156.762(7)
M4-O2A	2.1329(4)	2.0747(6)	M4′-O2A	2.3784(7)	2.4149(7)
M4-O2B	2.1403(3)	2.2021(5)	M4′-O2B	2.3552(8)	2.4154(8)
M4-O4A	2.2130(5)	2.1595(5)	M4′-O4A	2.4033(7)	2.4827(6)
M4-O4B	2.0697(4)	2.1292(4)	M4′-O4B	1.9479(6)	1.8923(8)
M4-O6A	2.5133(5)	2.4529(6)	M4′-O6A	2.3795(8)	2.3834(6)
M4-O5B	2.9412(4)	2.9051(6)	M4′-O5B	2.7684(8)	2.6692(7)
M4-O6B	2.9503(6)	3.0472(5)	M4′-O6B	2.6199(6)	2.5842(8)
<[5]M4-O>	2.2138	2.2037	<[5]M4′-O>	2.2929	2.3177

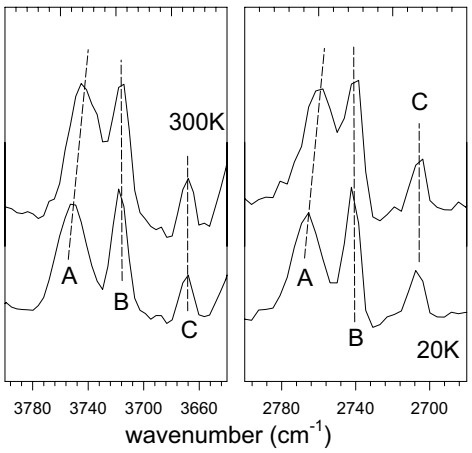

FIGURE 3. (**a**) OD- and (**b**) OH-stretching spectra of the studied amphibole at 298 and 20 K. The band labels are indicated.

of *b*-type reflections ($h + k = 2n + 1$) in the neutron-diffraction patterns. The same conclusion is provided by the IR spectra.

The cell edges show a similar decrease from 298 to 8 K (Table 2), with a slightly larger reduction shown by the *b* and *c* cell-edges. The absence of significant distortion of the unit cell is also reflected by the very minor change in the β angle (~0.1%, Table 2).

As the monoclinic symmetry constrains only one of the principal strain vectors to coincide with the lattice parameters (**b**), the orientation of the thermoelastic strain ellipsoid was calculated with the program STRAIN (Ohashi 1982) (Fig. 4). The principal unit-strain tensor components determined from the lattice parameters at room temperature and 8 K, are $|\varepsilon 1| = 5.1(8)\cdot10^{-6}$, $|\varepsilon 2| = 8.4(10)\cdot10^{-6}$, and $|\varepsilon 3| = 9.9(11)\cdot10^{-6}$ K^{-1}. The thermoelastic behavior seems more anisotropic ($\varepsilon 1:\varepsilon 2:\varepsilon 3 = 1.00:1.65:1.94$). The major axis of the strain ellipsoid ($\varepsilon 3$) at 8 K is oriented 40.8(9)° with respect to **c** (Fig. 4).

The results obtained here can be compared with the single-crystal SC-XRD data of Cámara et al. (2003) who studied (up to 643 K) a synthetic sample (sample 334) with a composition

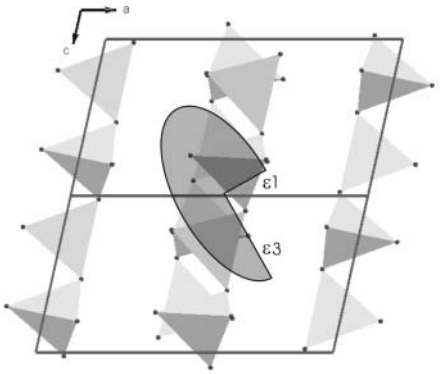

FIGURE 4. The thermoelastic unit-strain ellipsoid for the studied amphibole between room temperature and 8 K. The major axis of the strain ellipsoid (ε3) at 8 K is oriented 40.8(9)° with respect to **c**. Note: ε2 ∥ **b**, ∠(ε1^**b**)= ∠(ε3^**b**) = 90°, ∠(ε1^**c**)= 90° – ∠(ε3^**c**), ∠(ε1^**a**) = 90° – ∠(ε3^**a**), ∠(ε3^**a**) = ∠(ε3^**c**) + β

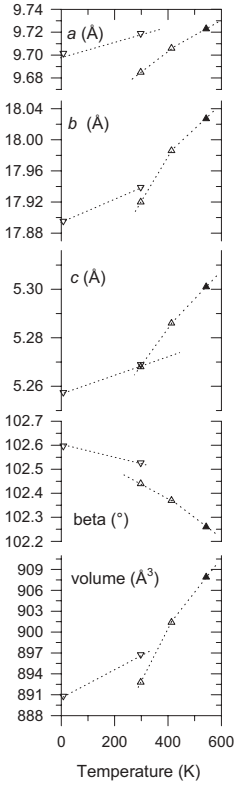

FIGURE 5. Comparison of the cell parameters obtained in this work (downward triangles) with the data of sample 334 (upward triangles) of Cámara et al. (2003). Filled triangle: sample 334 after the $P2_1/m \rightarrow C2/m$ phase-transition. The dashed lines are drawn as a guide to the eye. The *a* cell-edge difference is due to the partial A site vacancy of sample 334 (see text).

$[Na_{0.82}(Na_{0.81}Mg_{1.19})Mg_5Si_8O_{22}(OH)_2]$ very close to that of the amphibole studied here. Therefore the results obtained in these two studies can be confidently merged to gain further insight on the structural variations of this amphibole composition in a

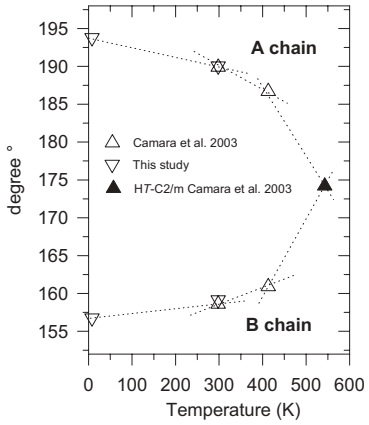

FIGURE 6. Change in the O5-O6-O5 angles between 8 and 573 K. Downward triangles: this study; upward triangles: Camara et al. (2003). Filled triangle: sample 334 after the $P2_1/m \rightarrow C2/m$ phase transition. The dashed lines are drawn as a guide to the eye.

temperature range in excess of 600 K and over 500 K for the same polymorph.

The variations in cell parameters are shown in Figure 5. The differences between the room-*T* data for *a*, *b*, and β is due to slight differences in composition between the studied samples. In fact sample 334 (Cámara et al. 2003) has a partial vacancy of the A site of about 0.2 apfu, balanced by an equal amount of Mg in the B site, whereas the sample of this study has less than 0.1 apfu of A site vacancy, again balanced by Mg in the B site.

It is worth noting that the *c* edge, which is mainly controlled by the T-site occupancy, is identical for both sets of data (Fig. 5). One difference seen in Figure 5 is the less steep trend displayed by the cell parameters of this study compared with those of Cámara et al. (2003) over a similar range of temperature (Fig. 5).

Cámara et al. (2003) found increases, from 298 to 573 K, of the M1, M2, M3, and M4 octahedral dimensions (given as the average M-O mean bond length) of 0.4, 0.6, 0.6, and 6%, respectively. The greater variation of M4-O with *T* is due to the change in coordination number of the B cation due to the *P-C* transition. In contrast, we observe here that the same octahedra reduce their volume by 0.1, 0.4, 0.2, and 0.5%, respectively. We conclude that the M1 and M3 octahedra are more rigid than the M2 site in response to decreasing *T*. If we extrapolate <M4-O> for the primitive polymorph of sample 334 of Cámara et al. (2003) (up to about 530 K), we note an expansion of 1%. Conversely, from 298 to 8 K, the reduction of the average bond length compared to the former is one-half (Table 4).

Combining our data with that of Cámara et al. (2003) over a similar temperature range, we can monitor the kinking of the A and B tetrahedral chains between 8 and 573 K (Fig. 6). At room *T*, the O5A-O6A-O5A and O5B-O6B-O5B angles obtained by neutron powder diffraction and SC-XRD refinement are virtually identical. At 573 K, the symmetry is *C*2/*m* and the double chains are equivalent and both extended, with the O5-O6-O5 angle ~174°. With decreasing *T*, down to 298 K, the amphibole converts to $P2_1/m$ and the chains are no longer equivalent; the A-chain lengthens as a function of decreasing *T* (the O5A-O6A-O5A angle increases to 189.9°) while the B-chain shrinks (the O5B-

O6B-O5B angle decreases to 158.6°) (Cámara et al. 2003).

The neutron data collected here show that with a further decrease in *T* to 8 K, the independent chains keep the same trend found for sample 334 (Cámara et al. 2003). However the rate of variation of the degree of chain kinking is less steep from room *T* to low *T*, than from room *T* to high *T* (Table 4 and Fig. 6). No intra-crystalline exchange was detected by neutron diffraction (and also by HT single-crystal diffraction). Thus, the separation of the A and B IR OH- and OD-stretching bands from ambient condition down to 8 K can only be due to differences in the topological configuration of the two non-equivalent tetrahedral rings.

ACKNOWLEDGMENTS

J.R. Smyth and R. Oberti gave helpful suggestions during manuscript preparation. This study was carried out during the stay of G.I. and G.D.G. at the Bayerisches Geoinstitut, financially supported by a Sofja Kovalevskaja grant, awarded to T. Boffa-Ballaran. D. Krausse assisted with the EPMA work. F.C. Hawthorne and D. M. Jenkins are kindly acknowledgment for their manuscript reviews. We also thank M. Fechtelkord for the editorial handling. The Forschungszentrum Jülich (Germany) and the ISIS Facility of the Rutherford Appleton Laboratory (U.K.) are acknowledged for neutron data collection through the respective European large scales facility access programmes.

REFERENCES CITED

Arlt, T. and Angel, R.J. (2000) Displacive phase transitions in *C*-centerd clinopyroxenes: spodumene, $LiScSi_2O_6$ and $ZnSiO_3$. Physics and Chemistry of Minerals, 27, 719–731.

Cámara, F., Oberti, R., Iezzi, G., and Della Ventura, G. (2003) The $P2_1/m \leftrightarrow C2/m$ phase transition in synthetic amphibole $Na(NaMg)Mg_5Si_8O_{22}(OH)_2$: thermodynamic and crystal-chemical evaluation. Physics and Chemistry of Minerals, 30, 570–581.

Della Ventura, G., Robert, J.-L., Hawthorne, F.C., and Prost, R. (1996) Short-range disorder of Si and Ti in the tetrahedral double-chain unit of synthetic Ti-bearing potassium-richterite. Amercian Mineralogist, 81, 56–60.

Dollase, W.A. (1986) Correction of intensities for preferred orientation in powder diffractometry: Application of the march model. Journal of Applied Crystallography, 19, 267–272.

Gaillard, F. (2004) Laboratory measurements of electrical conductivity of hydrous and dry silicic melts under pressure. Earth and Planetary Science Letters, 218, 215–228.

Hawthorne, F.C. (1983) The crystal chemistry of amphiboles. Canadian Mineralogist, 21, 173–480.

Iezzi, G., Della Ventura, G., Oberti, R., Cámara, F., and Holtz, F. (2004) Crystal-structure and crystal-chemistry of the synthetic $P2_1/m$ amphibole $Na(NaMg)Mg_5Si_8O_{22}(OH)_2$. American Mineralogist, 89, 640–646.

Larson, A.C. and Von Dreele, R.B. (1997) GSAS: General Structure Analysis System. Document LAUR 86-748, Los Alamos National Laboratory, New Mexico, USA.

Ohashi, Y. (1982) A program to calculate the strain tensor from two sets of unit cell parameters. In R.M. Hazen and L.W. Finger, Eds., Comparative Crystal Chemistry, 92–102. Wiley, New York.

Origlieri, M.J., Downs, R.T., Thompson, R.M., Pommier, C.J.S., Denton, M.B., and Harlow, G.E. (2003) High-pressure crystal structure of kosmochlor, $NaCrSi_6O_6$, and systematics of anisotropic compression in pyroxenes. American Mineralogist, 88, 1025–1032.

Pouchou, J.L. and Pichoir, F. (1985) 'PAP' $\Phi(\rho Z)$ procedure for improved quantitative micro-analysis. Microbeam Analysis, 104, 160.

Redhammer, G.J., Roth, G., Paulus, W., André, G., Lottermoser, W., Amthauer, G., Treutmann, W., and Koppelhuber-Bitschnau, B. (2001) The crystal and magnetic structure of Li-aegirine $LiFeSi_2O_6$: A temperature-dependent study. Physics and Chemistry of Minerals, 28, 337–346.

Rinaldi, R. (2002) Neutron scattering in mineral sciences: Preface. European Journal of Mineralogy, 14, 195–202.

Sato, A., Osawa, T., and Ohashi, H. (1995) Low-temperature form of $LiGaSi_2O_6$. Acta Crystallographica, C51, 1959–1960.

Thompson, J.B. (1970) Geometrical possibilities for amphibole structures: model biopyriboles. American Mineralogist, 55, 292–293.

Tribaudino, M., Nestola, F., Prencipe, M., and Rundolf, H. (2003) A single-crystal neutron-diffraction investigation of spodumene at 54 K. Canadian Mineralogist, 41, 521–527.

Yang, H. and Prewitt, C.T. (2000) Chain and layer silicates at high temperature and pressures. In High-temperature and high-pressure crystal chemistry, Reviews in Mineralogy, 41, 211–255. The Mineralogical Society of America, Washington, D.C.

Yang, H. and Smyth, J.R. (1996) Crystal structure of $P2_1/m$ ferromagnesian cummingtonite at 140 K. American Mineralogist, 81, 363–368.

MANUSCRIPT RECEIVED JULY 12, 2004
MANUSCRIPT ACCEPTED OCTOBER 19, 2004
MANUSCRIPT HANDLED BY MICHAEL FECHTELKORD